Probabilistic Engineering Mechanics 31 (2013) 1–11

Contents lists available at SciVerse ScienceDirect

Probabilistic Engineering Mechanics

journal homepage: www.elsevier.com/locate/probengmech

Stochastic reduced order models for random vectors: Application to random eigenvalue problems

James E. Warner*, Mircea Grigoriu, Wilkins Aquino [1]

School of Civil and Environmental Engineering, Cornell University, Ithaca, NY 14850, USA

ARTICLE INFO

Article history:
Received 17 November 2011
Received in revised form
23 July 2012
Accepted 23 July 2012
Available online 4 August 2012

Keywords:
Stochastic reduced order models
Uncertainty quantification
Random eigenvalue problem
Modal frequencies
Uncertain dynamic systems

ABSTRACT

An improved optimization algorithm is presented to construct accurate reduced order models for random vectors. The stochastic reduced order models (SROMs) are simple random elements that have a finite number of outcomes of unequal probabilities. The defining SROM parameters, samples and corresponding probabilities, are chosen through an optimization problem where the objective function quantifies the discrepancy between the statistics of the SROM and the random vector being modeled. The optimization algorithm proposed shows a substantial improvement in model accuracy and significantly reduces the computational time needed to form SROMs, as verified through numerical comparisons with the existing approach. SROMs formed using the new approach are applied to efficiently solve random eigenvalue problems, which arise in the modal analysis of structural systems with uncertain properties. Analytical bounds are established on the discrepancy between exact and SROM-based solutions for these problems. The ability of SROMs to approximate the natural frequencies and modes of uncertain systems as well as to estimate their dynamics in time is illustrated through comparison with Monte Carlo simulation in numerical examples.

1. Introduction

All physical systems and their corresponding computational models have inherent associated randomness. In practice, this uncertainty manifests itself in the input data (material properties, boundary or initial conditions, etc.) to a deterministic simulation that describes a particular physical system. Understanding and quantifying the impact of uncertainty on the simulation results is critical for successfully characterizing the system response. Despite advances in the field of stochastic computation, it remains a challenge to accurately and efficiently propagate uncertainty in computational models. Generally speaking, this is the problem of characterizing the statistics of the output $\mathbf{Y} \in \mathcal{Y} \subset \mathbb{R}^{d'}$ to a given forward mapping:

$$\mathcal{M} : \mathcal{X} \mapsto \mathcal{Y} \tag{1}$$

with random input parameters $\mathbf{X} \in \mathcal{X} \subset \mathbb{R}^{d}$. We note that models depending on random fields can also be described by this general form after an appropriate parameterization.

The most common and general approach to the solution to Eq. (1) is Monte Carlo simulation. Monte Carlo is non-intrusive and simple to implement, but due to its slow convergence it becomes infeasible for computationally intensive mappings $\mathcal{M}$. Variants such as Latin hypercube sampling and quasi-Monte Carlo sampling have been developed to accelerate convergence, but their applicability is often limited [15]. Intrusive approaches such as perturbation methods, operator-based methods (Neumann expansions), and the method of moments are among common non-sampling techniques. An inherent drawback of these methods is that they are difficult to implement for complex systems and are limited to problems with small magnitudes of uncertainties. Two techniques developed more recently based on generalized polynomial chaos (gPC) expansions [16], the stochastic Galerkin method [2] and the stochastic collocation method [1] have achieved success in several applications [5,10–12]. Stochastic collocation is non-intrusive and therefore easier to implement than the stochastic Galerkin method, but its computational cost grows rapidly with the dimension of the random input.

As a general alternative to these approaches, stochastic reduced order models (SROMs) were introduced in [7] and subsequently applied to determine effective conductivity for random microstructures and to calculate statistics of the states of linear dynamic systems in [8,9], respectively. A SROM $\tilde{\mathbf{X}}$ of a random input $\mathbf{X}$ is a random element with a finite and small number of samples which in general are not equally likely. The defining parameters of the SROM, its range and corresponding probabilities, are selected through an optimization problem with an objective function measuring the discrepancy between the statistics of $\tilde{\mathbf{X}}$ and $\mathbf{X}$. Although the ability of SROMs to efficiently solve stochastic problems like Eq. (1) has been demonstrated, the algorithm

* Corresponding author. Tel.: +1 607 255 3438; fax: +1 607 255 9004.
E-mail addresses: jw666@cornell.edu (J.E. Warner), mdg12@cornell.edu (M. Grigoriu), wa27@cornell.edu, wa20@duke.edu (W. Aquino).
[1] Current address: School of Civil and Environmental Engineering, Duke University, Durham, NC 27708, USA.

0266-8920/$ - see front matter © 2012 Elsevier Ltd. All rights reserved.
http://dx.doi.org/10.1016/j.probengmech.2012.07.001

employed for SROM construction in these works is suboptimal in that it considers only a finite search space for optimum parameters and results in the need to solve several reduced optimization problems in sequence.

In this work, we propose an improved optimization algorithm for constructing SROMs that results in models that are both formed more efficiently and provide a more accurate representation of the random vector being modeled. The approach is described in detail and then compared with the existing method in a numerical example illustrating the significant improvement in computational efficiency and accuracy achieved. The performance of SROMs formed with the new algorithm is demonstrated in the solution of random eigenvalue problems with application to modal analysis of structural systems with uncertain properties. We develop analytical bounds on SROM-based solutions to these problems. Furthermore, the ability to approximate the natural frequencies and modes of uncertain systems as well as to estimate their dynamics in time using SROMs is then demonstrated in numerical examples.

Section 2 introduces SROMs and describes both the construction of the models and how they are applied to obtain solutions to general stochastic problems. The newly proposed and existing SROM optimization algorithms are compared and contrasted here. In Section 3, the random eigenvalue problem is formulated and bounds are established on the discrepancy between SROM-based and exact solutions. Section 4 presents results from three numerical examples solved using SROMs. Finally, conclusions are drawn on the effectiveness of the new SROM optimization algorithm and the performance of SROMs for stochastic problems in Section 5.

2. Stochastic reduced order models (SROMs)

Let $(\Omega,\mathcal{F},P)$ and $(\Psi,\mathcal{G})$ denote a probability space and a measurable space, respectively. A function $X:\Omega\mapsto\Psi$ is a random element if it is measurable from $(\Omega,\mathcal{F})$ to $(\Psi,\mathcal{G})$, that is, if $X^{-1}(G)=\{\omega:X(\omega)\in G\}\in\mathcal{F}\ \forall G\in\mathcal{G}$ [6]. In our discussion, $\Psi=\mathbb{R}^d$ and $\mathcal{G}=\mathcal{B}(\mathbb{R}^d)$ is the Borel σ-algebra on $\mathbb{R}^d$, and so $\mathbf{X}:\Omega\mapsto\mathbb{R}^d$ is a d-dimensional random vector. We will assume that the probability law of $\mathbf{X}$ is fully specified with known expressions for its joint distribution, joint moments, and correlation matrix:

$$F(\mathbf{x})=P\left(\bigcup_{i=1}^{d}X_i\le x_i\right) \tag{2}$$

$$\mu(q_1,\ldots,q_d)=E\left[\prod_{i=1}^{d}X_i^{q_i}\right] \tag{3}$$

$$\mathbf{r}=E[\mathbf{X}\mathbf{X}^T] \tag{4}$$

provided the moments of order $q_1+\cdots+q_d$ in Eq. (3) exist and are finite for integers $q_i\ge 0$, $i=1,\ldots,d$. Similarly, the expressions for the marginal distributions and moments of order q are denoted as

$$F_i(x_i)=P(X_i\le x_i) \tag{5}$$

$$\mu_i(q)=E[X_i^q] \tag{6}$$

2.1. Generalities on SROMs

A stochastic reduced order model (SROM) $\tilde{\mathbf{X}}$ for $\mathbf{X}$ is a simple random element with a finite set of samples $\{\tilde{\mathbf{x}}^{(1)},\ldots,\tilde{\mathbf{x}}^{(m)}\}$ and corresponding probabilities $(p^{(1)},\ldots,p^{(m)})$ such that $p^{(k)}\ge 0\ \forall k$ and $\sum_{k=1}^{m}p^{(k)}=1$ [8]. Hence, the SROM $\tilde{\mathbf{X}}$ is completely defined by the model size m and sample-probability pairs $(\tilde{\mathbf{x}}^{(k)},p^{(k)}),k=1,\ldots,m$. With these SROM parameters specified, the distributions and moments of $\tilde{\mathbf{X}}$ corresponding to those of $\mathbf{X}$ given in Eqs. (2)–(6) are

$$\tilde{F}(\mathbf{x})=\sum_{k=1}^{m}p^{(k)}\mathbf{1}(\mathbf{x}\in R^{(k)}) \tag{7}$$

$$\tilde{\mu}(q_1,\ldots,q_d)=\sum_{k=1}^{m}p^{(k)}\left(\prod_{i=1}^{d}(\tilde{x}_i^{(k)})^{q_i}\right) \tag{8}$$

$$\tilde{r}(i,j)=\sum_{k=1}^{m}p^{(k)}\tilde{x}_i^{(k)}\tilde{x}_j^{(k)} \tag{9}$$

$$\tilde{F}_i(x_i)=\sum_{k=1}^{m}p^{(k)}\mathbf{1}(\tilde{x}_i^{(k)}\le x_i) \tag{10}$$

$$\tilde{\mu}_i(q)=\sum_{k=1}^{m}p^{(k)}(\tilde{x}_i^{(k)})^q \tag{11}$$

where $R^{(k)}=\times_{i=1}^{d}[\tilde{x}_i^{(k)},\infty)$ is a rectangle in $\mathbb{R}^d$ and $\mathbf{1}(\cdot)$ is the indicator function. Throughout this study, the shorthand notation used when referring to the SROM samples or probabilities is $\{\tilde{\mathbf{x}}\}$ and $\mathbf{p}$, respectively, in place of $\{\tilde{\mathbf{x}}^{(k)}\}_{k=1}^{m}=\{(\tilde{x}_1^{(1)},\ldots,\tilde{x}_d^{(1)}),\ldots,(\tilde{x}_1^{(m)},\ldots,\tilde{x}_d^{(m)})\}$ and $(p^{(1)},\ldots,p^{(m)})$.

2.2. SROM construction

According to the definition in the previous section, any m samples of $\mathbf{X}$ with probabilities summing to unity define a SROM $\tilde{\mathbf{X}}$. For practical purposes, however, we seek an optimal reduced order representation of $\mathbf{X}$ by imposing the condition that $\tilde{\mathbf{X}}$ and $\mathbf{X}$ have similar probability laws. Hence, for a given model size m, we choose the defining SROM parameters $\{\tilde{\mathbf{x}}\}$ and $\mathbf{p}$ as the solution to an optimization problem where the objective function quantifies the discrepancy between statistics of $\tilde{\mathbf{X}}$ and $\mathbf{X}$. In this study, we consider an objective function with three components representing differences between SROM and target marginal distributions, marginal moments up to order $\overline{q}\ge 1$, and correlation matrices

$$e_1(\{\tilde{\mathbf{x}}\},\mathbf{p})=\frac{1}{2}\sum_{i=1}^{d}\int_{I_i}(\tilde{F}_i(x_i)-F_i(x_i))^2\,dx_i \tag{12}$$

$$e_2(\{\tilde{\mathbf{x}}\},\mathbf{p})=\frac{1}{2}\sum_{i=1}^{d}\sum_{q=1}^{\overline{q}}\left(\frac{\tilde{\mu}_i(q)-\mu_i(q)}{\mu_i(q)}\right)^2 \tag{13}$$

$$e_3(\{\tilde{\mathbf{x}}\},\mathbf{p})=\frac{1}{2}\sum_{i,j=1;j>i}^{d}\left(\frac{\tilde{r}(i,j)-r(i,j)}{r(i,j)}\right)^2 \tag{14}$$

where I_i denotes the support of F_i and the SROM statistics $\tilde{F}_i(x_i)$, $\tilde{\mu}_i(q)$, and $\tilde{r}(i,j)$ have been defined in Eqs. (9)–(11).

The optimization problem for the construction of $\tilde{\mathbf{X}}$ is stated as follows:

$$\tilde{\mathbf{X}}\equiv\arg\min_{\{\tilde{\mathbf{x}}\},\mathbf{p}}\left(\sum_{i=1}^{3}\alpha_i e_i(\{\tilde{\mathbf{x}}\},\mathbf{p})\right)$$
$$\text{s.t.}\ \sum_{k=1}^{m}p^{(k)}=1\quad\text{and}\quad p^{(k)}\ge 0,\quad k=1,\ldots,m \tag{15}$$

where $\{\alpha_i\ge 0\}_{i=1}^{3}$ are weighting factors to ensure that each error component have similar order of magnitude or to emphasize the SROM's ability to represent a particular statistic of $\mathbf{X}$. For example, we can set $\alpha_1\gg\alpha_2,\alpha_3$ if the marginal distributions of $\mathbf{X}$ need to be represented accurately for a particular application. Note that the

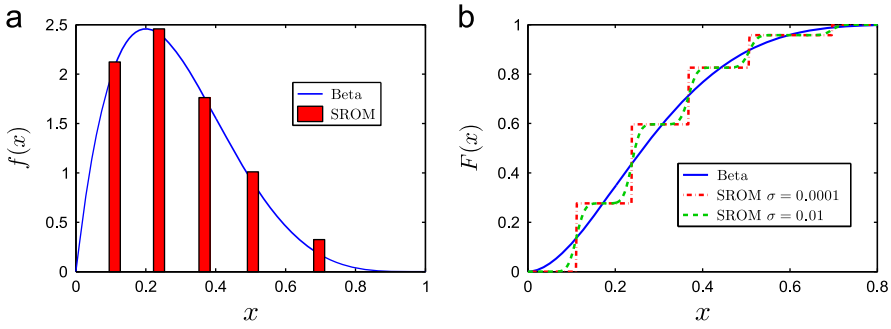

Fig. 1. Comparison of the pdf (a) and CDF (b) of the original beta distribution ($\alpha=2,\beta=5$) and the SROM formed by solving Eq. (15) with $m=5$. Note: the SROM probabilities in (a) are scaled such that $\max(\mathbf{p})=\max\{\text{beta pdf}\}$ for illustration.

model size m is not included in the optimization and is selected beforehand based on computational considerations.

In order to motivate a new approach to SROM construction, we now outline the simplified algorithm for solving the SROM optimization problem in Eq. (15) as proposed in [8,9]. First, a collection of n independent samples $\{\mathbf{x}^{(1)},\ldots,\mathbf{x}^{(n)}\}$ of $\mathbf{X}$ is generated and stored. It is assumed that n is large enough to accurately characterize the probability law of $\mathbf{X}$. Then, N_X distinct trial subsets of size m are drawn from $\{\mathbf{x}^{(1)},\ldots,\mathbf{x}^{(n)}\}$. For each trial subset, the optimization problem in Eq. (15) is solved for $\mathbf{p}$ while holding the trial samples constant. The defining SROM range $\{\tilde{\mathbf{x}}\}$ is chosen as the trial subset with the smallest optimal value of $\mathbf{e}(\{\tilde{\mathbf{x}}\},\mathbf{p})$ and the SROM probabilities are set to the corresponding optimum values of $\mathbf{p}$. It is noted that this existing approach is suboptimal since (1) the search space for optimum SROM samples $\{\tilde{\mathbf{x}}\}$ is limited to a finite set, (2) only a relatively small number N_X of subsets of the original set are examined, and (3) the defining SROM parameters $\{\tilde{\mathbf{x}}\}$ and $\mathbf{p}$ are determined sequentially rather than jointly.

In this study we look to achieve improved SROM performance by optimizing over $\{\tilde{\mathbf{x}}\}$ and $\mathbf{p}$ jointly rather than sequentially. In doing so, the ability of $\tilde{\mathbf{X}}$ to accurately represent $\mathbf{X}$ benefits from a search over the entire probability space for SROM samples rather than being limited to a finite subset. In addition to increased accuracy, we also seek to reduce the computation time required for SROM construction. By combining the selection of the defining SROM parameters into one algorithm run, significant computational speedup is expected over the existing approach where N_X reduced optimization problems must be solved.

In order to facilitate the use of efficient gradient-based optimization algorithms, closed-form expressions for derivatives of the objective function with respect to the SROM parameters are now derived. Due to the presence of discontinuities in the SROM cumulative distribution function (CDF) given by Eq. (10), we must utilize a smooth approximation to $\tilde{F}(x)$ with well-defined derivatives. For this, we use

$$\tilde{F}(x)\approx\tilde{F}^s(x;\sigma)=\sum_{k=1}^{m}\frac{1}{2}p^{(k)}\left(1+\operatorname{erf}\left(\frac{x-\tilde{x}^{(k)}}{\sqrt{2}\sigma}\right)\right) \tag{16}$$

where $\operatorname{erf}(x)$ is the Gauss error function:

$$\operatorname{erf}(x)=\frac{2}{\sqrt{\pi}}\int_0^x e^{-t^2}\,dt \tag{17}$$

Note that we have introduced an additional free parameter σ which controls the degree of smoothing present in $\tilde{F}^s(x;\sigma)$. It can be easily verified that the approximate CDF $\tilde{F}^s$ is monotone increasing, right-continuous, and satisfies $\lim_{x\to-\infty}\tilde{F}^s(x)=0$ and $\lim_{x\to+\infty}\tilde{F}^s(x)=1$. Furthermore, $\tilde{F}^s$ becomes equal to the original CDF $\tilde{F}$ as $\sigma\to0$. The smoothed CDF, however, has the advantage that its derivative with respect to a given SROM sample is well-defined. That is,

$$\frac{\partial\tilde{F}^s}{\partial\tilde{x}_j}=-\frac{p_j}{\sqrt{2\pi\sigma^2}}\exp\left(-\frac{1}{2\sigma^2}(x-\tilde{x}_j)^2\right) \tag{18}$$

Substituting $\tilde{F}^s$ for $\tilde{F}$ in the CDF error component e_1, explicit expressions for the derivatives of the objective function in (15) with respect to the SROM parameters can be derived as

$$\begin{aligned}\frac{\partial}{\partial\tilde{x}_n^{(l)}}[e(\{\tilde{\mathbf{x}}\},\mathbf{p})]&=-\alpha_1\frac{p^{(l)}}{\sqrt{2\pi\sigma^2}}\int_{I_n}\left(\tilde{F}_n^s(x_n)-F(x_n)\right)\\&\times\exp\left(-\frac{1}{2\sigma^2}(x_n-\tilde{x}_n^{(l)})^2\right)dx_n+\alpha_2\sum_{q=1}^{\bar{q}}\left(\frac{\tilde{\mu}_q(n)-\mu_q(n)}{\mu_q(n)^2}\right)(qp^{(l)}(\tilde{x}_n^{(l)})^{q-1})\\&+\alpha_3\sum_{i,j=1;j>i}^{d}(\tilde{r}(i,j)-r(i,j))p^{(l)}(\delta_{in}\tilde{x}_j^{(l)}+\delta_{jn}\tilde{x}_i^{(l)})\end{aligned} \tag{19}$$

$$\begin{aligned}\frac{\partial}{\partial p^{(l)}}[e(\{\tilde{\mathbf{x}}\},\mathbf{p})]&=\alpha_1\frac{1}{2}\sum_{i=1}^{d}\int_{I_i}(\tilde{F}_i^s(x_i)-F(x_i))\left(1+\operatorname{erf}\left(\frac{x_i-\tilde{x}_i^{(l)}}{\sqrt{2}\sigma}\right)\right)dx_i\\&+\alpha_2\sum_{i=1}^{d}\sum_{q=1}^{\bar{q}}\left(\frac{\tilde{\mu}_q(i)-\mu_q(i)}{\mu_q(i)^2}\right)(\tilde{x}_i^{(l)})^q+\alpha_3\sum_{i,j=1;j>i}^{d}(\tilde{r}(i,j)-r(i,j))(\tilde{x}_i^{(l)}\tilde{x}_j^{(l)})\end{aligned} \tag{20}$$

where δ_{ij} is the Kronecker delta.

We note that the most computationally intensive part of the SROM optimization problem defined in (15) is the numerical evaluation of the integral appearing in the CDF error term e_1 and its corresponding derivatives. This cost can become especially prohibitive when the CDF support is large or as d and m are increased. Therefore, for larger scale problems, we replace the integral in Eq. (12) with a summation and evaluate the CDF error pointwise to speed up the optimization using

$$\bar{e}_1=\frac{1}{2}\sum_{i=1}^{d}\sum_{j=1}^{m}(\tilde{F}_i^s(\tilde{x}_i^{(j)})-F_i(\tilde{x}_i^{(j)}))^2 \tag{21}$$

We mention that in this case a relatively inaccurate SROM CDF $\tilde{F}_i^s(x)$ may yield a small value for $\bar{e}_1$ and so in practice it can be necessary to increase the value of α_1 in Eq. (15) to offset this effect.

2.2.1. Example: beta random variable

In this subsection, the proposed optimization algorithm is used to construct a SROM for a random variable described by a beta probability distribution. The purpose of this simple example is to demonstrate the ability of a SROM with small model size to represent a given random variable and to compare the accuracy and computational efficiency of the new and previously proposed optimization algorithms. To implement the new approach, the derivatives in Eqs. (19) and (20) are supplied to a gradient-based

optimization algorithm in MATLAB [13] for the minimization of the objective function in (15). Constraints requiring $p^{(k)} \geq 0$, $k = 1, \ldots, m$, and $\sum_{k=1}^{m} p^{(k)} = 1$ are specified.

The probability density function (pdf) of the beta distribution is

$$f(x;\alpha,\beta) = \frac{x^{\alpha-1}(1-x)^{\beta-1}}{B(\alpha,\beta)}, \quad x \in I = (0,1) \tag{22}$$

where $B(\cdot,\cdot)$ is the beta function and it can be seen that the distribution is fully described by two shape parameters α and β. We examine the SROM for the case where $(\alpha,\beta) = (2,5)$. The size of the SROM is specified as $m = 5$. We consider moments up to order five ($\overline{q} = 5$) in the moment error component e_2 (Eq. (13)). The qth moment of a beta random variable is computed as

$$\mu_q = E[X^q] = \frac{B(\alpha+q,\beta)}{B(\alpha,\beta)} \tag{23}$$

The CDF and moment error components of the objective function are given equal weight ($\alpha_1 = \alpha_2 = 1$) while the correlation error component is not present in the 1D case. The initial guess for the optimization is five independently mmdrawn samples from the beta distribution with equal probability $p = 1/m = 0.2$.

The results from the construction of the beta random variable SROM using the newly proposed algorithm are shown in Fig. 1 and Table 1. In Fig. 1(a), the true beta pdf is plotted verse a bar graph illustrating the defining SROM samples and probabilities chosen via the optimization problem. Note that the height of the bars representing the probability of each sample are scaled such that $\max(\mathbf{p}) = \max\{\text{beta pdf}\}$ for illustration purposes. Fig. 1(b) compares the true beta CDF and the SROM CDF as computed by Eq. (16) for the optimum SROM parameters and two different values of the smoothing parameter σ. It is noted that the optimization was performed separately for each value of σ and yielded nearly identical SROM parameters. The percent error between the SROM moments computed by Eq. (11) and the true moments given in (23) are displayed in Table 1. It is seen that the error is well below 1% for all five moments and less than 0.1% for the 4th and 5th moments.

In order to compare the performance of the SROM optimization algorithm with the approach proposed in [8], we now construct a SROM for the beta random variable using this existing framework. All problem parameters specified above remain unchanged. Recall that in this approach the SROM probabilities $\mathbf{p}$ are chosen to minimize Eq. (15) for N_X trial subsets of independent samples of X. The subset that results in the smallest objective function value is chosen as the SROM range $\{\tilde{x}\}$. Here, we store the optimum objective function value and CPU time taken to complete the optimization for $N_X = 1:1000$. For comparative purposes, we assume the group of N_X trial subsets is grown as N_X increases by first randomly drawing a new subset of size m and then adding it to the previously selected subsets. In this way, we record a new optimum objective function value only when the current subset results in the smallest observed value thus far. Similarly, the CPU time for the current value of N_X is computed as the sum of times for all the previous optimization trials. Due to the random nature of the algorithm, three trials of this experiment are performed and compared with results generated using the new joint optimization approach.

The results comparing CPU times and accuracy of SROMs formed using both optimization algorithms are shown in Fig. 2(a) and (b), respectively. The solid line displaying CPU time for the new algorithm (2.16 s) is taken as the average from five optimization runs with randomly selected initial SROM ranges. The final objective function value shown in Fig. 2(b) was the same in each trial. Fig. 2(a) shows that the existing algorithm takes more CPU time to carry out except in the case of considering only a very small number of trial subsets ($N_X \lesssim 7$). For the value of N_X where the CPU times are roughly equal, it can be seen in Fig. 2(b) that the optimum objective function value obtained by the new algorithm is about two orders of magnitude smaller than that of the existing algorithm. The figure also shows that none of the three trials of the existing algorithm achieves the same degree of accuracy as the new algorithm when considering up to 1000 trial subsets. It is further noted that the existing algorithm takes over 100 times longer to perform the optimization when $N_X = 1000$.

The results shown in this section demonstrate the ability of a SROM to provide a satisfactory representation of a random variable with just a small number of defining parameters. Through comparisons with the existing approach, it is seen that the optimization algorithm proposed here for SROM construction provides a substantial improvement in performance. By expanding the search space for the SROM samples from a finite set to the entire support and optimizing jointly over both samples and probabilities, the new algorithm shows a 100-fold improvement in speed and accuracy in this example. The suboptimal performance of the existing algorithm is most likely a consequence of the SROM range being chosen as independently drawn samples of X. Thus, the samples tend to be clustered in highly likely regions of the range of X without adequate representation for less probable areas. Optimum samples chosen via the new optimization algorithm, however, are seen to be evenly spread throughout the entire support of X in the results presented.

Table 1
SROM moment errors for the beta random variable example.

Moment order	1	2	3	4	5
% Error	0.592	0.244	0.292	0.016	0.074

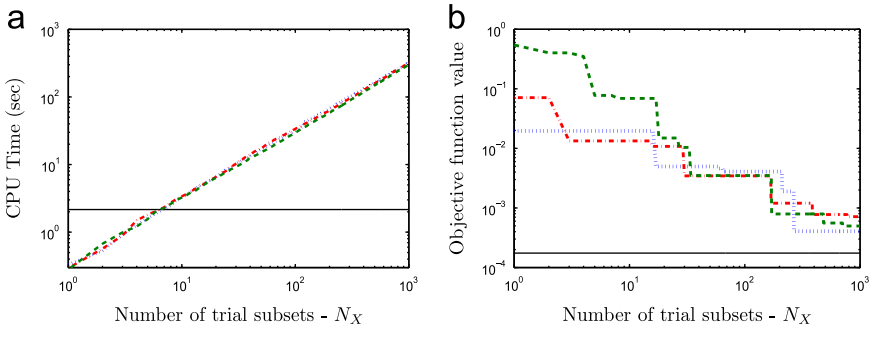

Fig. 2. Comparison of the performance of the new SROM optimization algorithm (solid line) versus three trials of the approach proposed in [8] (dashed lines). (a) compares the computation time taken to solve the optimization problem in Eq. (15), while (b) compares the final objective function value obtained through each algorithm.

Table 2
Maximum and minimum percent error for five trials of Monte Carlo moment estimates ($n=5$) for the beta random variable example.

Moment order	1	2	3	4	5
Min. % error	4.17	8.82	2.01	1.63	7.14
Max. % error	31.11	60.25	92.13	126.28	159.91

2.3. Solutions by SROMs

For a general stochastic problem given in Eq. (1), our goal is to use SROMs to efficiently characterize the statistics of the output $\mathbf{Y}\in\mathcal{Y}\subset\mathbb{R}^{d'}$ given the probability law of the random input $\mathbf{X}\in\mathcal{X}\subset\mathbb{R}^{d}$ and a deterministic mapping $\mathcal{M}$. The construction of a SROM $\tilde{\mathbf{Y}}$ from which the statistics of $\mathbf{Y}$ can be estimated involves two steps. First, a SROM $\tilde{\mathbf{X}}$ is formed for the input $\mathbf{X}$ through the solution of the optimization problem in Eq. (15). Second, the range for $\tilde{\mathbf{Y}}$ is obtained by evaluating the forward mapping m times with $\mathbf{X}=\tilde{\mathbf{x}}^{(k)}$:

$$\mathcal{M}:\tilde{\mathbf{x}}^{(k)}\mapsto\tilde{\mathbf{y}}^{(k)},\quad k=1,\ldots,m \tag{24}$$

This range $\{\tilde{\mathbf{y}}\}$ along with the original set of input SROM probabilities $\mathbf{p}$ define the output SROM $\tilde{\mathbf{Y}}$. The marginal distributions and moments of $\mathbf{Y}$ can then be estimated as

$$E[Y_i^q]\approx E[\tilde{Y}_i^q]=\sum_{k=1}^{m}p^{(k)}(\tilde{y}_i^{(k)})^q \tag{25}$$

$$P(Y_i\le\xi)\approx P(\tilde{Y}_i\le\xi)=\sum_{k=1}^{m}p^{(k)}\mathbf{1}(\tilde{y}_i^{(k)}\le\xi) \tag{26}$$

From Eqs. (24)–(26) it can be seen that the SROM solution to a stochastic problem requires m forward solves corresponding to the samples of $\tilde{\mathbf{X}}$ which have unequal probability in general. Contrast this with traditional Monte Carlo solutions, which require n forward solves corresponding to independent, equally likely samples of $\mathbf{X}$. It was seen in the previous example that a 1D beta random variable could be accurately represented by a SROM with just $m=5$ samples. For comparison, the first five moments of the beta random variable with $(\alpha,\beta)=(2,5)$ are estimated using Monte Carlo with $n=5$ samples. The maximum and minimum percent errors are computed for five different Monte Carlo trials and displayed in Table 2. The moment estimates are both highly inaccurate and unstable as one may expect when using so few samples.

As we will see in later sections, satisfactory SROM-based solutions to random eigenvalue problems are obtained for $m\le 20$. The advantage of SROM solutions over Monte Carlo for these problems and stochastic problems in general is that they are accurate and stable for $m\ll n$ samples. Thus, a SROM-based approach to Eq. (1) requires far fewer evaluations of $\mathcal{M}$ but has added overhead for forming the input SROM $\tilde{\mathbf{X}}$. In this light, the benefits in efficiency become more pronounced for computationally intensive forward problems and problems with lower dimensional inputs. Thus, the same stored input SROM can be used to efficiently solve multiple stochastic problems for different combinations of any deterministic problem parameters.

3. Random eigenvalue problems by SROMs

In this study, the SROM solution framework is applied to stochastic eigenvalue problems defined by matrices with random entries. A particular application where this problem arises is the modal analysis of structural systems in which the elements of the system have uncertain stiffness given by the components of a random vector $\mathbf{X}\in\mathbb{R}^{d}$. Here, one is interested in determining the modal frequencies whose squares are the solution to the generalized eigenvalue problem

$$[K]\{\mathbf{V}\}=\Lambda[M]\{\mathbf{V}\} \tag{27}$$

where $M\in\mathbb{R}^{d'\times d'}$ and $K\in\mathbb{R}^{d'\times d'}$ are the system mass and stiffness matrix, respectively, and $\mathbf{V}\in\mathbb{R}^{d'}$ is an eigenvector and Λ is an eigenvalue. Since the entries of K are random, so are the modal frequencies of the system. We note that since our intended application is the analysis of discrete structural systems for which the mass matrix is diagonal, the generalized eigenvalue problem in Eq. (27) reduces to a standard eigenvalue problem in practice. Hence, it will suffice to focus on the problem of estimating a set of eigenvalues $\mathbf{\Lambda}=(\Lambda_1,\ldots,\Lambda_{d'})$ corresponding to an arbitrary symmetric matrix K with random entries.

As described in Section 2.3, the statistics of the solution to this stochastic eigenvalue problem can be estimated by forming a reduced order model $\tilde{\mathbf{\Lambda}}$ for the eigenvalues $\mathbf{\Lambda}$. After a SROM $\tilde{\mathbf{X}}$ is formed for $\mathbf{X}$, the construction of $\tilde{\mathbf{\Lambda}}$ requires the solution of m deterministic eigenvalue problems defined by $\tilde{k}^{(k)}=K(\tilde{x}^{(k)})$, $k=1,\ldots,m$. The statistics of $\mathbf{\Lambda}$ are then approximated using Eqs. (25) and (26). In this section we study the accuracy of SROM approximations of random eigenvalues by developing analytical bounds on the discrepancy between SROM and exact eigenvalue solutions. In the subsequent applications section, the accuracy of SROM-based eigenvalue solutions are verified numerically through the modal analysis of two different structural systems.

3.1. Accuracy of SROM-based solutions

The relative accuracy of the SROM $\tilde{\mathbf{X}}$ can be evaluated straightforwardly by using the objective function $\mathbf{e}(\{\tilde{\mathbf{x}}\},\mathbf{p})$ as a metric. The performance of the SROM $\tilde{\mathbf{\Lambda}}$ for $\mathbf{\Lambda}$, however, depends on both the discrepancy between $\tilde{\mathbf{X}}$ and $\mathbf{X}$ and the mapping $\mathbf{X}\mapsto\mathbf{\Lambda}$. Hence, the SROM $\tilde{\mathbf{\Lambda}}$ corresponding to an accurate $\tilde{\mathbf{X}}$ can be unsatisfactory because of the complexity of this mapping. To gauge the performance of $\tilde{\mathbf{\Lambda}}$, we develop bounds on the discrepancy between $\tilde{\mathbf{\Lambda}}$ and $\mathbf{\Lambda}$ that depend on both the accuracy of $\tilde{\mathbf{X}}$ and the mapping $\mathbf{X}\mapsto\mathbf{\Lambda}$. To do so, we first obtain bounds on the discrepancy between eigenvalues of two distinct deterministic matrices. The bounds are then extended to the case of matrices with random entries in the following subsection.

3.1.1. Deterministic eigenvalue bounds

Consider the following deterministic eigenvalue problems:

$$A\mathbf{v}=\lambda\mathbf{v} \tag{28}$$

$$\hat{A}\hat{\mathbf{v}}=\hat{\lambda}\hat{\mathbf{v}} \tag{29}$$

where $A,\hat{A}\in\mathbb{R}^{d'\times d'}$ and we define the matrix $D\equiv\hat{A}-A$ as a finite perturbation to A. Our objective is to bound the discrepancy between the eigenvalues of A and $\hat{A}$ in terms of the size of the perturbation D. Given that the main application considered involves finding natural frequencies and modes of stochastic linear dynamic systems that result from symmetric eigenvalue problems, it will suffice to focus on bounds case where A and D are symmetric. It is well known that these bounds are tighter and more informative than the general non-symmetric case. Two bounds are stated here: the first addresses the difference in the whole set of d' eigenvalues of $\hat{A}$, while the second addresses the difference in one particular eigenvalue.

First bound (*Wielandt–Hoffman theorem*): If $(\lambda_1,\ldots,\lambda_{d'})$ and $(\hat{\lambda}_1,\ldots,\hat{\lambda}_{d'})$ are the eigenvalues of the symmetric matrices A and

$\hat{A}=A+D$, respectively, then

$$\sum_{i=1}^{d'}(\hat{\lambda}_i-\lambda_i)^2 \leq \|D\|_F^2 \tag{30}$$

where $\|\cdot\|_F$ is the Frobenius norm. The proof can be found in Section 3 of [14].

Second bound (*Weyl's theorem*): If $(\lambda_1,\ldots,\lambda_{d'})$ and $(\hat{\lambda}_1,\ldots,\hat{\lambda}_{d'})$ are the eigenvalues of the symmetric matrices A and $\hat{A}=A+D$, respectively, then

$$|\hat{\lambda}_k-\lambda_k| \leq \|D\|_2 \tag{31}$$

for $k=1:d'$. Or equivalently

$$\max_k |\hat{\lambda}_k-\lambda_k| \leq \|D\|_2 \tag{32}$$

The proof can be found in Section 5.2 of [4].

3.1.2. Stochastic eigenvalue bounds

The deterministic eigenvalue bounds presented previously are now used to provide measures of accuracy on SROM-based solutions to stochastic eigenvalue problems. We begin with bounds on the discrepancy between the SROM eigenvalue estimate $\tilde{\boldsymbol{\Lambda}}$ and corresponding Monte Carlo approximation, denoted as $\widehat{\boldsymbol{\Lambda}}$. For the purpose of this exposition, let us suppose we have a collection of independent samples $\{\mathbf{x}^{(i)}\}_{i=1}^n$ of $\mathbf{X}$. Here, it is assumed that n is large enough to characterize the probability law of $\mathbf{X}$ satisfactorily. Let $\tilde{\mathbf{X}}$ be a SROM of size $m \ll n$ defined by samples $\{\tilde{\mathbf{x}}^{(k)}\}_{k=1}^m$ and probabilities $(p^{(1)},\ldots,p^{(m)})$. We make the simplifying assumption that $\{\tilde{\mathbf{x}}^{(k)}\}_{k=1}^m$ are a subset of the Monte Carlo samples $\{\mathbf{x}^{(i)}\}_{i=1}^n$.

First, we would like to bound the difference in eigenvalue solutions corresponding to a single Monte Carlo and SROM sample using the deterministic bounds in Section 3.1.1. We assume K is a symmetric matrix whose entries are a function of the components of $\mathbf{X}$. Let $\mathcal{K}^{(i)}$ and $\tilde{\mathcal{K}}^{(k)}$ denote two versions of this matrix formed corresponding to the Monte Carlo sample $\mathbf{x}^{(i)}$ and the SROM sample $\tilde{\mathbf{x}}^{(k)}$, respectively. If $\boldsymbol{\lambda}^{(i)}$ are the eigenvalues corresponding to $\mathcal{K}^{(i)}$ and $\tilde{\boldsymbol{\lambda}}^{(k)}$ are the eigenvalues corresponding to $\tilde{\mathcal{K}}^{(k)}$, we can use Eq. (30) to bound the discrepancy in these sets of eigenvalues as

$$\|\tilde{\boldsymbol{\lambda}}^{(k)}-\boldsymbol{\lambda}^{(i)}\|_2 \leq \|\tilde{\mathcal{K}}^{(k)}-\mathcal{K}^{(i)}\|_F \tag{33}$$

where we have let $D=\tilde{\mathcal{K}}^{(k)}-\mathcal{K}^{(i)}$ be the perturbation matrix in this case. Similarly, if we are concerned with the discrepancy between one eigenvalue in particular, we can use Eq. (31) to write

$$|\tilde{\lambda}_j^{(k)}-\lambda_j^{(i)}| \leq \|\tilde{\mathcal{K}}^{(k)}-\mathcal{K}^{(i)}\|_2 \tag{34}$$

We now introduce a partition to the collection of samples $\{\mathbf{x}^{(i)}\}_{i=1}^n$ in order to use (33) and (34) to derive bounds on $E[\|\tilde{\boldsymbol{\Lambda}}-\widehat{\boldsymbol{\Lambda}}\|_2]$ and $E[|\tilde{\Lambda}_j-\widehat{\Lambda}_j|]$. Denote this partition as $\{\mathcal{I}_k, k=1,\ldots,m\}$ where each set $\mathcal{I}_k$ contains n_k samples and has a nuclei at the SROM sample $\tilde{\mathbf{x}}^{(k)}$. Samples from $\{\mathbf{x}^{(i)}\}_{i=1}^n$ are placed in a given cluster $\mathcal{I}_k$ by attempting to approximately satisfy two conditions: (1) $\mathbf{x}^{(i)}$ is closer to $\tilde{\mathbf{x}}^{(k)}$ than any other $\tilde{\mathbf{x}}^{(l)}$, $l\neq k$, and (2) $p^{(k)}=n_k/n$ for $k=1,\ldots,m$. In this way, the Monte Carlo samples of $\mathbf{X}$ that comprise $\mathcal{I}_k$ all have similar spatial proximity to $\tilde{\mathbf{x}}^{(k)}$ and the probability that $\mathbf{X}$ is represented by a sample that lies in cluster $\mathcal{I}_k$ is $n_k/n \approx p^{(k)}$. An algorithm to construct a partition with these properties was proposed in [8].

With such a partition in place, we can compute $E[\|\tilde{\boldsymbol{\Lambda}}-\widehat{\boldsymbol{\Lambda}}\|_2]$ as a weighted average of this discrepancy in each cluster of the partition

$$\begin{aligned} E[\|\tilde{\boldsymbol{\Lambda}}-\widehat{\boldsymbol{\Lambda}}\|_2] &= \sum_{k=1}^m p^{(k)}\left(\frac{1}{n_k}\sum_{\mathbf{x}^{(i)}\in\mathcal{I}_k}\|\tilde{\boldsymbol{\lambda}}^{(k)}-\boldsymbol{\lambda}^{(i)}\|_2\right) \\ &\approx \frac{1}{n}\sum_{k=1}^m\sum_{\mathbf{x}^{(i)}\in\mathcal{I}_k}\|\tilde{\boldsymbol{\lambda}}^{(k)}-\boldsymbol{\lambda}^{(i)}\|_2 \\ &\leq \frac{1}{n}\sum_{k=1}^m\sum_{\mathbf{x}^{(i)}\in\mathcal{I}_k}\|\tilde{\mathcal{K}}^{(k)}-\mathcal{K}^{(i)}\|_F \end{aligned} \tag{35}$$

where we have used $p^{(k)}\approx n_k/n$ in the second equality and the bound in (33) for the final inequality. The same arguments can be made for $|\tilde{\Lambda}_j-\widehat{\Lambda}_j|$. Consequently, we have that the moments of order q of $\|\tilde{\boldsymbol{\Lambda}}-\widehat{\boldsymbol{\Lambda}}\|_2$ and $|\tilde{\Lambda}_j-\widehat{\Lambda}_j|$ satisfy the following inequalities:

$$E[\|\tilde{\boldsymbol{\Lambda}}-\widehat{\boldsymbol{\Lambda}}\|_2^q] \leq \frac{1}{n}\sum_{k=1}^m\sum_{\mathbf{x}^{(i)}\in\mathcal{I}_k}(\|\tilde{\mathcal{K}}^{(k)}-\mathcal{K}^{(i)}\|_F)^q \tag{36}$$

$$E[|\tilde{\Lambda}_j-\widehat{\Lambda}_j|^q] \leq \frac{1}{n}\sum_{k=1}^m\sum_{\mathbf{x}^{(i)}\in\mathcal{I}_k}(\|\tilde{\mathcal{K}}^{(k)}-\mathcal{K}^{(i)}\|_2)^q \tag{37}$$

We note that as $m\to n$, the radius of each set $\mathcal{I}_k$ approaches zero. As a result, each $\mathcal{I}_k$ contains only its nucleus $\tilde{\mathbf{x}}^{(k)}$ and $n_k\to 1$. Hence, the SROM-based solution approaches the Monte Carlo solution in this limit case since both use the same samples of $\mathbf{X}$ and the probabilities $p^{(k)}$ converge to $1/n$.

With regard to an exact solution $\boldsymbol{\Lambda}$ to a stochastic eigenvalue problem, we can characterize the discrepancy of the SROM-based approximation $\tilde{\boldsymbol{\Lambda}}$ as

$$E[\|\tilde{\boldsymbol{\Lambda}}-\boldsymbol{\Lambda}\|_2^q] \leq E[\|\tilde{\boldsymbol{\Lambda}}-\widehat{\boldsymbol{\Lambda}}\|_2^q]+E[\|\widehat{\boldsymbol{\Lambda}}-\boldsymbol{\Lambda}\|_2^q] \tag{38}$$

Since $\tilde{\boldsymbol{\Lambda}}$ approaches $\widehat{\boldsymbol{\Lambda}}$ as $m\to n$ and Monte Carlo estimates $\widehat{\boldsymbol{\Lambda}}$ converge to $\boldsymbol{\Lambda}$ as $n\to\infty$, we can see that the expectation of the difference between $\boldsymbol{\Lambda}$ and $\tilde{\boldsymbol{\Lambda}}$ converges to 0 in this limit case. We note that while the relative performance of two distinct input SROMs $\tilde{\mathbf{X}}$ can be effectively gauged by comparing the optimum objective function values in Eq. (15) corresponding to each model, the bounds in Eqs. (36)–(38) provide less explicit information on the quality of SROM solutions $\tilde{\boldsymbol{\Lambda}}$. These bounds are less sharp in the sense that they do not address convergence rate and because the asymptotic convergence argument above is not as useful in practice since $m \ll n$ in general. Development of analytical measures on the rates of convergence of $\tilde{\boldsymbol{\Lambda}}$ to $\boldsymbol{\Lambda}$ is beyond the scope of this study.

4. Applications

The SROM solution framework is now applied in several numerical examples. We demonstrate the performance of SROM-based solutions to stochastic eigenvalue problems through two examples involving the modal analysis of uncertain structural systems. The first analyzes a simple shear-frame idealization of a structure while the second considers a more general planar frame model. For the shear-frame model, we also consider the uncertain dynamics of the system and use SROMs to estimate the statistics of its evolution in time. We conclude the section with a numerical example illustrating one of the open research issues associated with the SROM-based approach to stochastic problems.

4.1. Shear-frame model

Consider a structure with N_s stories modeled by a planar frame of width $2L$ and height N_{sL}. In this section, we examine the highly idealized case where the beams of the structure are assumed to be rigid and we neglect both the joint rotations and the axial

deformation of the beams and columns. These assumptions result in the shear-frame or shear-beam model commonly used in structural engineering [3]. The mass is idealized as concentrated at the floor levels and thus there are N_s degrees of freedom $(U_1,\ldots,U_{N_s})$ corresponding to the relative horizontal motion of each lumped mass $\mathtt{M}$. Here, we assume the combined lateral stiffness of the columns connecting each story is uncertain and given by the components of the random vector $\mathbf{X}\in\mathbb{R}^d$ where $d=N_s$. The stiffness matrix for this simplified system is tridiagonal and has the general form

$$K=\begin{bmatrix} X_1+X_2 & -X_2 & \cdots & 0 \\ -X_2 & X_2+X_3 & \cdots & 0 \\ \vdots & \vdots & \ddots & -X_d \\ 0 & 0 & -X_d & X_d \end{bmatrix} \tag{39}$$

while the diagonal mass matrix is given by

$$M=\mathrm{diag}(\mathtt{M},\mathtt{M},\ldots,\mathtt{M}/2)\in\mathbb{R}^{d\times d} \tag{40}$$

Let us suppose that $\mathbf{X}$ is a translation random vector with coordinates

$$X_i=F^{-1}\circ\Phi(G_i),\quad i=1,\ldots,d, \tag{41}$$

where F is a shifted gamma distribution with shift, shape, and decay parameters $a=1$, $k=2$, and $\lambda=3$, respectively. The vector $\mathbf{G}=(G_1,\ldots,G_d)$ is an $\mathbb{R}^d$-valued Gaussian variable with coordinates G_i of mean 0, variance 1, and correlations given by

$$E[G_iG_j]=\rho^{|i-j|},\quad \rho\in[0,1] \tag{42}$$

4.1.1. Modal analysis

Our goal in this section is to estimate the statistics of the eigenvalues $\mathbf{\Lambda}=(\Lambda_1,\ldots,\Lambda_d)$ of the matrix $\hat{K}=M^{-1}K$ by forming the reduced model $\tilde{\mathbf{\Lambda}}$, as described in Section 3. We reiterate that these eigenvalues represent the square root of the system's modal frequencies. Using Eqs. (25) and (26) we compute the distribution and moment of order q of $\tilde{\Lambda}_i$ as $P(\tilde{\Lambda}_i\le\xi)=\sum_{k=1}^m p^{(k)}\mathbf{1}(\tilde{\lambda}_i^{(k)}\le\xi)$ and $E[\tilde{\Lambda}_i^q]=\sum_{k=1}^m p^{(k)}(\tilde{\lambda}_i^{(k)})^q$, respectively. We also seek mean estimates of the eigenvectors of $\hat{K}$ representing the modes of the shear-frame model. To gauge the accuracy of the SROM-based solutions, we compare with Monte Carlo solutions computed from 10,000 independent realizations of $\hat{K}$. It is noted that a similar problem is solved in [7] for the case when $d=3$. Here, we study the performance of the new optimization algorithm for larger scale problems by letting $d=10$.

The error metrics we use to quantify accuracy of the SROM solutions will be the maximum percent error in moments for each order, the average percent error in all moments, and the average absolute error in CDFs:

$$\epsilon_q=100\times\max_i\left[\frac{|E[\tilde{\Lambda}_i^q]-E[\Lambda_i^q]|}{E[\Lambda_i^q]}\right],\quad q=1,\ldots,\overline{q} \tag{43}$$

$$\overline{\epsilon}_M=100\times\left(\frac{1}{d'\overline{q}}\right)\sum_{i=1}^{d'}\sum_{q=1}^{\overline{q}}\left[\frac{|E[\tilde{\Lambda}_i^q]-E[\Lambda_i^q]|}{E[\Lambda_i^q]}\right] \tag{44}$$

$$\overline{\epsilon}_{CDF}=\frac{1}{d'}\sum_{i=1}^{d'}\int_{I_i}(\tilde{F}_{\tilde{\Lambda}_i}(\xi_i)-F_{\Lambda_i}(\xi_i))^2\,d\xi_i \tag{45}$$

Results are generated for the case when $\rho=0.5$ for three different SROM sizes $m=5$, 10, 20. We consider moments up to order $\overline{q}=4$ when forming the SROM $\tilde{\mathbf{X}}$ and set the weighting factors in Eq. (15) as $(\alpha_1,\alpha_2,\alpha_3)=(1e2,1,1)$. We choose a larger value for α_1 since we are evaluating the CDF error pointwise as in Eq. (21) and hence a small error value can be achieved even if the SROM CDF is relatively inaccurate. The smoothing parameter of the SROM CDF in all results is set as $\sigma=0.001$.

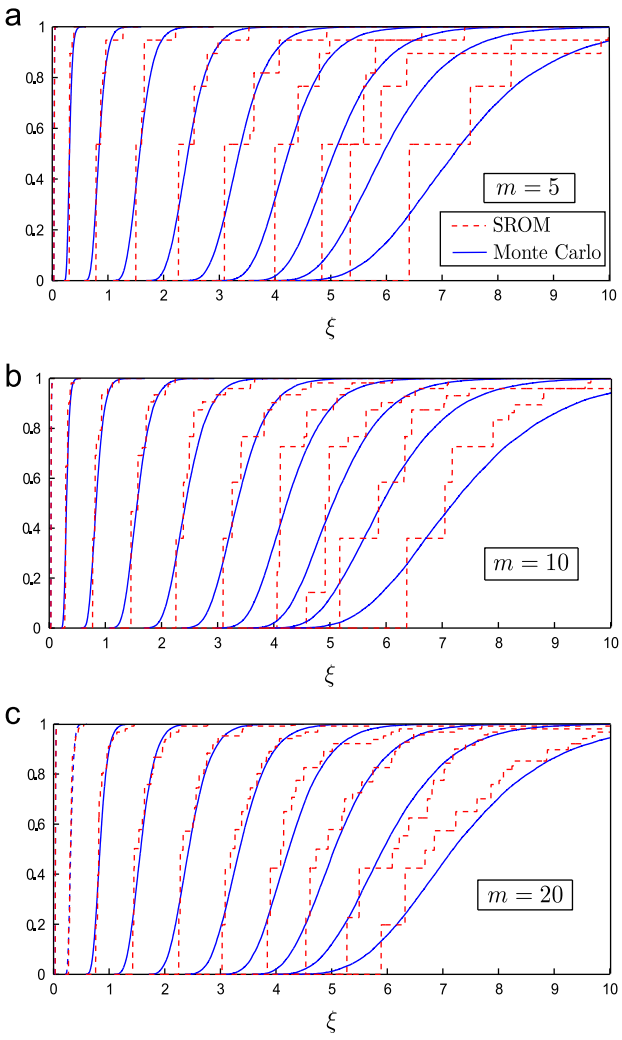

Fig. 3. Estimates of the distributions of $\Lambda_i, i=1,\ldots,10$ in Example 4.1.1. The SROM approximations (dashed line) for (a) $m=5$, (b) $m=10$, and (c) $m=20$ are compared with the Monte Carlo solution (solid line) using 10,000 samples.

Table 3
SROM moment and CDF errors as defined in Eqs. (43)–(45) for Example 4.1.1.

Model size (m)	ϵ_1	ϵ_2	ϵ_3	ϵ_4	$\overline{\epsilon}_M$	$\overline{\epsilon}_{CDF}$
5	2.81	5.17	9.36	14.44	4.02	2.60e−2
10	2.44	6.36	11.33	16.93	2.90	2.00e−2
20	3.18	6.40	10.09	13.99	2.71	1.25e−2

The distributions of $\tilde{\Lambda}_i$ and Λ_i as computed with Monte Carlo are compared in Fig. 3 for $m=5$, 10, 20. It is seen that we obtain accurate approximate distributions, even for a small model size of $m=5$. The accuracy is especially prominent for the lower order eigenvalues with smaller variance, and it improves, generally, as m increases. The SROM moment and CDF errors, as computed in Eqs. (43)–(45), are displayed in Table 3 for the different model sizes tested. The maximum moment errors remain similar for the different model sizes while the average moment and CDF errors decrease as m increases. We note that the maximum moment errors occur for each case in estimates of the largest system eigenvalue. We can see by the values of $\overline{\epsilon}_M$, however, that the error in each moment is typically much smaller than the maximum values observed. Fig. 4 shows the mean estimates of the eigenvectors of

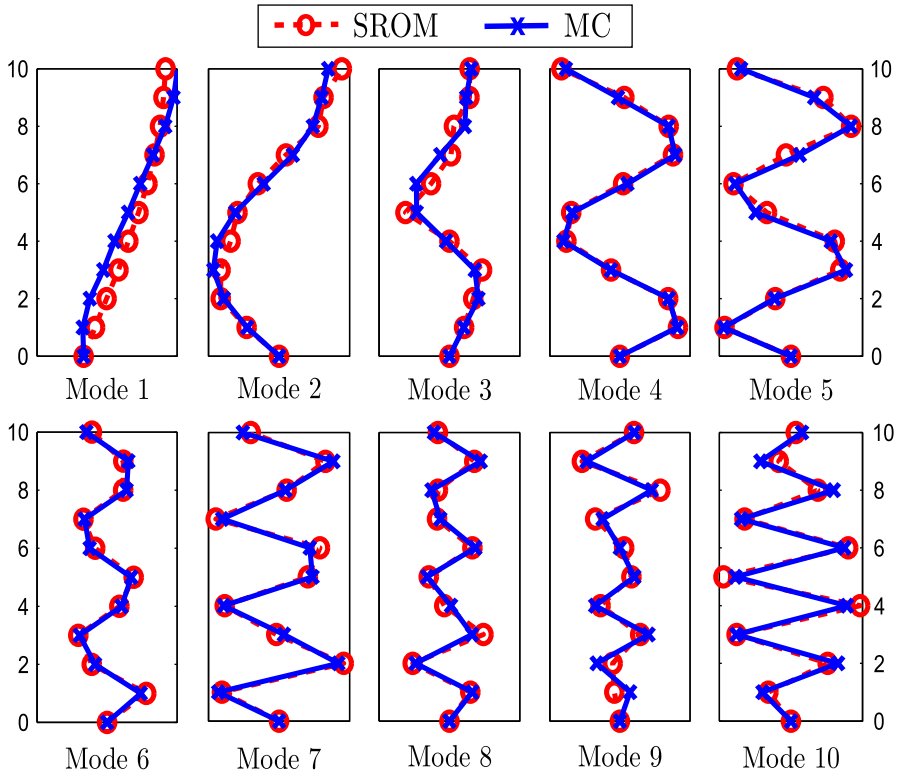

Fig. 4. Mean estimates for the modes in Example 4.1.1 computed using SROMs ($m=20$) and Monte Carlo (10,000 samples).

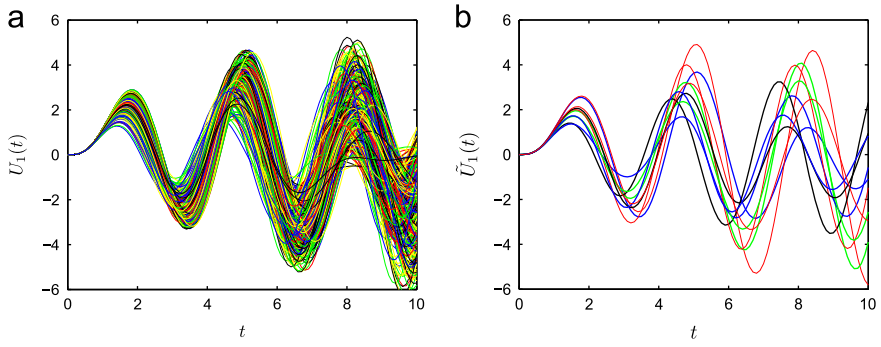

Fig. 5. Samples of $U_1(t)$ (a) and $\tilde{U}_1(t)$ (b).

$\hat{K}$ using both Monte Carlo and SROMs for the case when $m=20$, it is seen that the SROM estimates show excellent agreement.

4.1.2. *Uncertain dynamics*

In this section, we consider the dynamics of the shear-frame model with uncertain stiffness described above. We demonstrate the ability of SROMs to accurately estimate the statistics of the evolution of displacement in the structure in time under harmonic loading. The motion of the horizontal degrees of freedom $\mathbf{U}=(U_1,\ldots,U_{Ns})$ is governed by

$$M\ddot{\mathbf{U}}+C\dot{\mathbf{U}}+K\mathbf{U}=\mathbf{P} \tag{46}$$

where K and M for the shear frame are given in Eqs. (39) and (40), respectively. The damping matrix C is estimated using the Caughey damping model [3, Section 11.4.2] with a damping ratio of 5% prescribed for each of the system modes.

We examine the case where the structure has three stories ($N_s=3$) and again the floor stiffnesses are described by the shifted gamma distribution in Eq. (41) with the defining parameters unchanged from the previous section. We assume the frame is initially at rest when a force $P_1=5\sin(2t)$ is applied to the first story. Here, we seek the statistics of the motion of each degree of freedom from $t_0=0$ s to $t_f=10$ s. A SROM $\tilde{\mathbf{X}}$ of size $m=10$ is formed for $\mathbf{X}$ and the corresponding SROM $\tilde{\mathbf{U}}(t)$ of $\mathbf{U}(t)$ is constructed by solving Eq. (46) with $\mathbf{X}=\tilde{\mathbf{x}}^{(k)}, k=1,\ldots,m$. We compare the SROM-based solution with the Monte Carlo solution using 1000 independent samples of $\mathbf{X}$.

Fig. 5(a) shows 1000 independent Monte Carlo samples of the solution $U_1(t)$ representing the motion of the first degree of freedom. Fig. 5(b) shows the 10 samples $(\tilde{u}_1^{(1)}(t),\ldots,\tilde{u}_1^{(m)}(t))$ making up the range of $\tilde{U}_1(t)$ for comparison. The first four moments of $U_1(t)$ computed using the SROM $\tilde{U}_1(t)$ are plotted in Fig. 6 against the Monte Carlo estimates. The SROM-based approximations for each moment show excellent agreement and

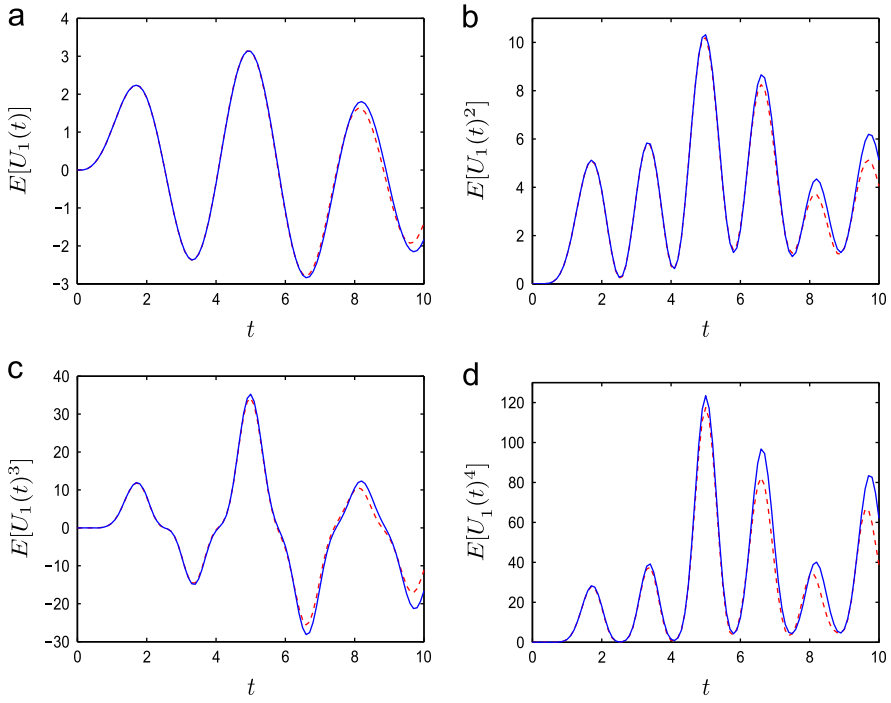

Fig. 6. Estimates of the first four moments of $U_1(t)$ computed using the SROM (dashed) and Monte Carlo (solid) in Example 4.1.2.

Table 4
SROM moment errors as defined in (47).

Order (q)	1	2	3	4
$i=1$	0.30	0.54	1.47	3.03
$i=2$	0.43	1.76	2.18	3.35
$i=3$	0.30	1.35	2.15	3.62

are nearly identical for $t<5$ s. To demonstrate the accuracy of the SROM-based moments for the remaining degrees of freedom, the percent error in each moment is computed using

$$\varepsilon_i(q) = 100 \times \frac{\int_{t_o}^{t_f} (E[U_i(t)^q] - E[\tilde{U}_i(t)^q])^2 \, dt}{\int_{t_o}^{t_f} (E[U_i(t)^q])^2 \, dt} \tag{47}$$

and is displayed in Table 4. It is seen that the error for moments up to order four in each degree of freedom is less than 4% while the error in the mean estimates is well below 1%.

4.2. Modal analysis of a general planar frame

In this example, we relax some of the simplifying assumptions made for the shear-frame model and consider a more general planar frame model of a structure with N_s stories. Specifically, we no longer assume that the beams in the frame are rigid and hence allow for non-zero joint rotations $(\theta_{1,1},\theta_{1,2},\ldots,\theta_{N_s,2})$ in addition to the horizontal displacements $(U_1,\ldots,U_{N_s})$. In doing so, we now allow the stiffness in each member of the frame to vary randomly rather than assigning one value to characterize the lateral stiffness of each level. For this analysis, we assign a value for Young's modulus of each member as

$$\mathcal{E}_i = a + bX_i, \quad i=1,\ldots,d \tag{48}$$

with $(a,b)=(2,3)$ and where X_i is given by Eq. (41) with F as a beta distribution having shape parameters $(\alpha,\beta)=(2,5)$. The components of $\mathbf{G}$ again have mean 0, variance 1, and correlations given by Eq. (42). We assume unit values for the moment of inertia in each member as well as the story height L and mass $\mathtt{M}$.

Table 5
SROM moment and CDF errors as defined in Eqs. (43)–(45) for Example 4.2.

ρ	**m**	ϵ_1	ϵ_2	ϵ_3	ϵ_4	$\overline{\epsilon}_M$	$\overline{\epsilon}_{CDF}$
0.2	10	15.00	14.49	13.17	5.38	4.10	3.35e−1
	20	15.26	3.77	17.30	11.87	3.46	1.09e−1
0.9	10	10.74	13.27	9.74	5.50	3.60	4.30e−1
	20	0.79	6.25	13.03	17.12	2.78	1.97e−1

Again, we are interested in the natural frequencies and mode shapes of this system through the solution of the eigenvalue problem in Eq. (27). For the general planar frame considered here, the mass and stiffness matrices can be partitioned as

$$M = \begin{bmatrix} M_{11} & 0 \\ 0 & 0 \end{bmatrix}, \quad K = \begin{bmatrix} K_{11} & K_{12} \\ K_{21} & K_{22} \end{bmatrix} \tag{49}$$

where the 11 and 22 blocks of the matrices correspond to the translational and rotational degrees of freedom, respectively. Through a static condensation procedure, Eq. (27) reduces to finding the eigenvalues $\mathbf{\Lambda}=(\Lambda_1,\ldots,\Lambda_{d'})$ of the matrix $\overline{K}=M_{11}^{-1}(K_{11}-K_{12}K_{22}^{-1}K_{21})$. We note that while M_{11} has the same form as Eq. (40), the stiffness matrix K lacks special structure and does not possess a straightforward expression in terms of an arbitrary number of stories in this case.

We examine the case where the frame has four stories and so $d=12$. Since we are neglecting rotational inertia, there are four frequencies and modes $(d'=4)$ corresponding to the structure's horizontal degrees of freedom. We generate results for SROM sizes $m=10,20$ and for correlation coefficients $\rho=0.2,0.9$ in Eq. (42). The objective function weights and smoothing parameter are assigned as $(\alpha_1,\alpha_2,\alpha_3)=(1e2,1,1)$ and $\sigma=0.001$, respectively. We once again employ the error metrics in Eqs. (43)–(45) to

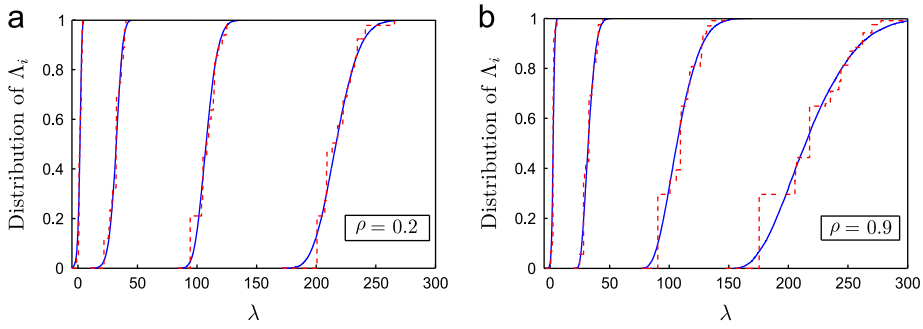

Fig. 7. Estimates of the distributions of $\Lambda_i, i=1,\ldots,4$ in Example 4.2. The SROM approximation (dashed line) with $m=20$ is compared with the Monte Carlo solution (solid line) using 10,000 samples for $\rho=0.2$ and $\rho=0.9$.

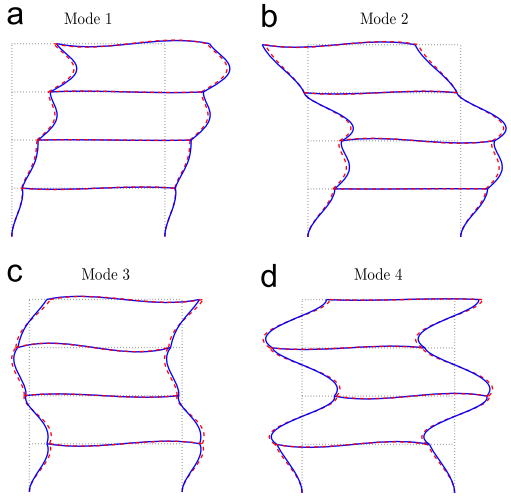

Fig. 8. Mean estimates for the modes of the planar frame in Example 4.2 computed using SROMs with $m=10$ (dashed line) and Monte Carlo with 10,000 samples (solid line) for the case when $\rho=0.9$. (a) Mode 1. (b) Mode 2. (c) Mode 3. (d) Mode 4.

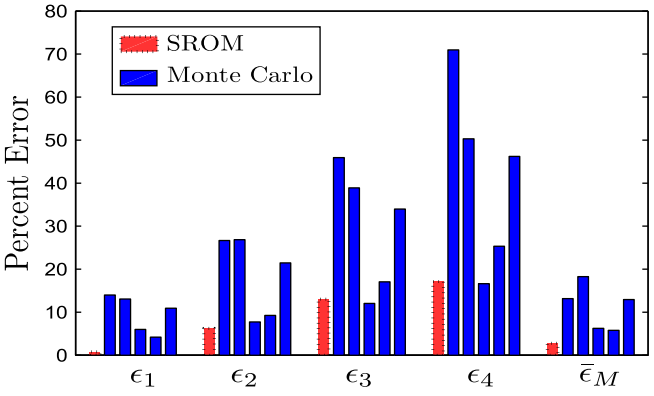

Fig. 9. Comparison of the accuracy of eigenvalue moment estimates in Example 4.2 using SROMs and five trials of Monte Carlo with the same number of samples ($m=n=20$). The maximum moment error (ϵ_i, $i=1,\ldots,4$) and average moment error($\bar{\epsilon}_M$) are defined in Eqs. (43) and (44), respectively.

gauge SROM accuracy using Monte Carlo simulation with 10,000 samples as the reference solution.

The errors in the SROM approximations for the moments and distributions of Λ_i are displayed in Table 5 for each combination of model size and correlation coefficient. It can be seen that the SROM estimates are more accurate for a higher correlation coefficient value and the average moment and CDF errors decrease for a larger model size m as expected. The decrease in error is more pronounced in the distribution estimates as the SROM size is increased from $m=10$ to $m=20$. The SROM estimates for the distributions of Λ_i with $m=20$ are compared with the Monte Carlo solution for the case of $\rho=0.2$ and $\rho=0.9$ in Fig. 7(a) and (b), respectively. The approximate distributions for each eigenvalue show excellent agreement in both cases. Finally, the mean estimates for the modes of the structure using SROMs can be seen in Fig. 8 for the case where $m=10$ and $\rho=0.9$. The approximate modes using SROMs are nearly identical to those computed using Monte Carlo with 10,000 samples.

For comparative purposes, the accuracy of eigenvalue moment estimates using Monte Carlo with 20 independent samples is examined. For $\rho=0.9$, we compute the percent moment errors defined in Eqs. (43) and (44) for five Monte Carlo trials. These results are shown in Fig. 9 in comparison to the SROM estimate with $m=20$ presented above. In contrast to the SROM moment estimates, the Monte Carlo approximations can have very large errors and the magnitude of these errors varies greatly across the different trials. For example, the average moment error $\bar{\epsilon}_M$ for the five Monte Carlo trials are 13.15%, 18.28%, 6.26%, 5.79%, and 12.95% compared with 2.78% for the SROM estimate.

4.3. Non-convexity of the SROM objective function

In this subsection, we demonstrate an open issue in the construction of SROMs for random vectors in that the objective function in Eq. (15) has many local minima. A plot of the objective function versus two components of a SROM sample in Fig. 10(a) shows its complexity. We illustrate the existence of distinct solutions resulting from local minima of the objective function by reexamining the example in Section 4.1.1 for three random starting points in the construction of $\tilde{\mathbf{X}}$. We let $d=3$ and $m=10$ and randomly draw the initial guess for the SROM samples according to Eq. (41) for each of the three trials. All other problem parameters remain fixed at previously specified values. We compare the final objective function values $\mathbf{e}$ obtained for each $\tilde{\mathbf{X}}$ as well as the accuracy of the three corresponding eigenvalue SROMs $\tilde{\mathbf{\Lambda}}$.

In Table 6, we see that indeed the three optimization trials forming $\tilde{\mathbf{X}}$ result in varying final objective function values. The average moment and CDF errors of the corresponding eigenvalue SROMs $\tilde{\mathbf{\Lambda}}$ are seen to vary as well. In the three trials shown, the average eigenvalue moment error increases as the objective function value increases but the same trend does not hold true with the CDF error. The distributions of $\tilde{\Lambda}_i$ and Λ_i for the three trials are compared in Fig. 10(b), again showing the distinction between each solution formed from different SROMs $\tilde{\mathbf{X}}$.

While this example confirms that SROM construction and resulting SROM-based solutions are sensitive to the initial guess provided, we observe that SROM parameters corresponding to local minima of Eq. (15) generally provide a satisfactory

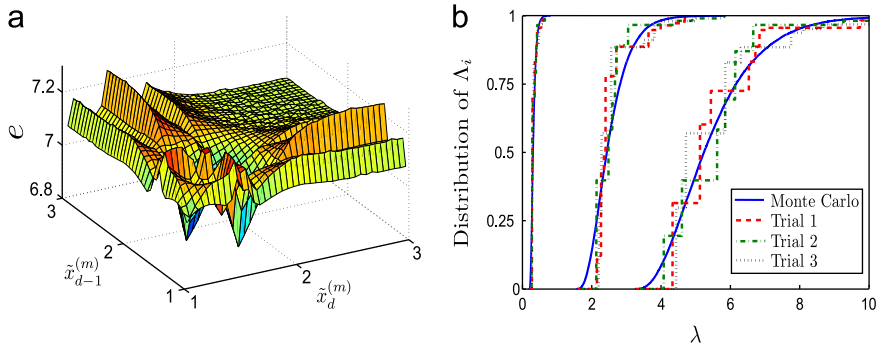

Fig. 10. (a) SROM objective function in Eq. (15) versus two components of a SROM sample. (b) Distribution of eigenvalues from Example 4.1.1 ($d=3$, $m=10$) for SROMs $\tilde{\mathbf{\Lambda}}$ corresponding to SROMs $\tilde{\mathbf{X}}$ formed from three optimization trials with different initial guesses.

Table 6
Objective function values **e** for SROMs $\tilde{\mathbf{X}}$ formed from three random initial guesses and the moment and CDF errors of the corresponding eigenvalue estimates provided by the SROMs $\tilde{\mathbf{\Lambda}}$ in Example 4.1.1.

Trial	**e**	$\overline{\epsilon}_M$	$\overline{\epsilon}_{CDF}$
1	8.95e−5	1.48	2.03e−2
2	4.58e−5	2.30	1.59e−2
3	4.40e−4	3.08	2.34e−2

representation of **X**. Indeed, the eigenvalue estimates provided by each of the three trials have an average error in moments of 3% or lower and the approximate distributions show excellent agreement with the Monte Carlo solution. Furthermore, we argue that the computational benefits of utilizing gradient-based optimization over global optimization techniques outweigh the potential trade-off in accuracy resulting from a local minimum solution. In practice, one can partially circumvent this issue by performing the optimization for several starting points and then using the most accurate SROM input to efficiently solve a particular forward problem. Depending on the application, this approach will still result in a significant computational speedup over traditional Monte Carlo simulation.

5. Conclusions

An improved approach has been proposed to construct stochastic reduced order models $\tilde{\mathbf{X}}$ for general random vectors **X**. The defining SROM parameters are obtained through the solution of an optimization problem where the objective function quantifies the discrepancy between marginal distributions, marginal moments, and correlation matrices of $\tilde{\mathbf{X}}$ and **X** with constraints on admissible values of the probabilities $(p^{(1)},\ldots,p^{(m)})$. The existing approach to SROM construction entails solving a series of reduced optimization problems for optimum probability values corresponding to different sets of independently drawn samples of **X**, which are held fixed in each trial. By optimizing jointly over both $\{\tilde{\mathbf{x}}^{(1)},\ldots,\tilde{\mathbf{x}}^{(m)}\}$ and $(p^{(1)},\ldots,p^{(m)})$ in one procedure, the optimization algorithm presented here displays significant improvement in computational efficiency and accuracy, as demonstrated through numerical comparisons with the simplified approach used previously.

SROMs formed using the proposed algorithm have been applied to provide efficient solutions to random eigenvalue problems that arise in the modal analysis of structural systems with uncertain properties. SROMs were also shown to provide accurate estimates of the dynamics of such uncertain systems in time. Analytical bounds were established on the discrepancy between exact and SROM-based solutions to random eigenvalue problems. Numerical examples show that SROM-based estimates for the statistics of natural frequencies and modes of dynamic systems with random stiffness are accurate and stable for small SROM sizes $m \lesssim 20$. On the other hand, Monte Carlo estimates with the same number of samples are unstable and can be highly inaccurate.

Acknowledgments

Wilkins Aquino and James Warner would like to thank the National Science Foundation (NSF) for its kind support through the grant CAREER-0643618. Mircea Grigoriu would like to thank NSF for its support through grants CMMI-0969150 and CMMI-0925714.

References

[1] Babuska I, Nobile F, Tempone R. A stochastic collocation method for elliptic partial differential equations with random input data. SIAM Journal of Numerical Analysis 2007;45(3):1005–34.
[2] Babuska I, Tempone R, Zouraris GE. Galerkin finite element approximations of stochastic elliptic partial differential equations. SIAM Journal of Numerical Analysis 2004;42:800–25.
[3] Chopra AK. Dynamics of structures: theory and applications to earthquake engineering2nd ed. Upper Saddle River, NJ: Prentice-Hall; 2001.
[4] Demmel JW. Applied numerical linear algebra. Philadelphia, PA: SIAM; 1997.
[5] Gottlieb D, Xiu D. Galerkin method for wave equations with uncertain coefficients. Communications in Computational Physics 2008;3(2):505–18.
[6] Grigoriu M. Stochastic calculus. Applications in science and engineering. Boston: Birkhäuser; 2002.
[7] Grigoriu M. Reduced order models for random functions. Application to stochastic problems. Applied Mathematical Modelling 2009;33:161–75.
[8] Grigoriu M. Effective conductivity by stochastic reduced order models (sroms). Computational Materials Science 2010;50:138–46.
[9] Grigoriu M. Linear random vibration by stochastic reduced-order models. International Journal for Numerical Methods in Engineering 2010;82:1537–59.
[10] Le Maitre O, Knio O, Najm H, Ghanem R. A stochastic projection method for fluid flow: basic formulation. Journal of Computational Physics 2001;173:481–511.
[11] Lin G, Wan X, Su C-H, Karniadakis GE. Stochastic computational fluid mechanics. IEEE Computing in Science and Engineering 2007;9(2):21–9.
[12] Marzouk Y, Xiu D. A stochastic collocation approach to Bayesian inference in inverse problems. Communications in Computational Physics 2009;6(4):826–47.
[13] MATLAB version 7.10.0 (R2010a). The MathWorks Inc., Natick, Massachusetts, 2010.
[14] Wilkinson JH. Elementary proof of the Wielandt–Hoffman theorem and of its generalization. Technical Report, Stanford University, Stanford, California; 1970.
[15] Xiu D. Numerical methods for stochastic computations. A spectral method approach. Princeton, NJ: Princeton University Press; 2010.
[16] Xiu D, Karniadakis GE. The Weiner–Askey polynomial chaos for stochastic differential equations. SIAM Journal of Scientific Computing 2002;24(2):619–44.